THE EUROPEAN
PHYSICAL JOURNAL C

CrossMark

Scaling properties of inclusive W± production at hadron colliders

François Arleo[1,a], **Émilien Chapon**[1,b], **Hannu Paukkunen**[2,3,4,c]

[1] Laboratoire Leprince-Ringuet, École polytechnique, CNRS/IN2P3, Université Paris-Saclay, 91128 Palaiseau, France
[2] Department of Physics, University of Jyvaskyla, P.O. Box 35, 40014 University of Jyvaskyla, Finland
[3] Helsinki Institute of Physics, P.O. Box 64, 00014 University of Helsinki, Finland
[4] Departamento de Física de Partículas and IGFAE, Universidade de Santiago de Compostela, 15782 Santiago de Compostela, Galicia, Spain

Abstract We consider the hadroproduction of W gauge bosons in their leptonic decay mode. Starting from the leading-order expressions, we show that by defining a suitable scaling variable the centre-of-mass dependence of the cross sections at the LHC energies can be essentially described by a simple power law. The scaling exponent is directly linked to the small-x behaviour of parton distribution functions (PDF) which, at the high virtualities involved in W production, is largely dictated by QCD evolution equations. This entails a particularly simple scaling law for the lepton charge asymmetry and also predicts that measurements in different collision systems (p–p, p–$\bar{\text{p}}$, p–Pb Pb–Pb) are straightforwardly related. The expectations are compared with the existing data and a very good overall agreement is observed. It is shown that the PDF uncertainty in certain cross-section ratios between nearby centre-of-mass energies can be significantly reduced by taking the ratios at fixed value of the scaling variable instead of fixed rapidity.

1 Introduction

The production of W gauge bosons in hadronic collisions is a process which is sensitive to practically all aspects of Standard Model, from electro-weak couplings to QCD dynamics and the non-perturbative parton content of the hadrons [1]. One of the most precisely measured observables at hadron colliders is the rapidity (y) dependence of the lepton charge asymmetry, $\mathcal{C}_\ell$,

$$\mathcal{C}_\ell(y) \equiv \frac{d\sigma^{\ell^+}/dy - d\sigma^{\ell^-}/dy}{d\sigma^{\ell^+}/dy + d\sigma^{\ell^-}/dy}, \qquad (1)$$

where the charged lepton ($\ell = e, \mu$) originates from the leptonic decay of the W boson. This observable is a useful probe of proton parton distribution functions (PDFs), in particular, to disentangle the flavour dependence [2–4] which is not well constrained by the deep inelastic scattering.[1] Today, the charge asymmetry has been studied in detail by the CDF [5,6] and D0 [7–10] experiments in p–$\bar{\text{p}}$ collisions at the Tevatron as well as the ATLAS [11,12], CMS [13,14], and LHCb [15,16] experiments in p–p collisions at the LHC. While the broad features of the experimental data are well captured by fixed-order perturbative QCD calculations [17,18], the simultaneous reproduction of the D0 data in bins of different kinematic cuts is known to pose difficulties [19–22].

The first measurements of W production in p–Pb collisions have recently appeared [23–25] and various observables seem to favour the use of EPS09 nuclear PDFs (nPDFs) [26] instead of a naive superposition of free nucleon PDFs (similar conclusion can be expected in the case of other sets of nPDFs [27–29]). In addition, these measurements may also help to probe, for the first time, the flavour dependence of nuclear modifications in quark densities [23]. The production of W bosons in heavy-ion collisions is also of paramount importance. Measurements by ATLAS [30] and CMS [31] in Pb–Pb collisions have revealed that the production rate approximately scales with the number of binary nucleon-nucleon collisions. This is in sharp contrast to hadronic observables (high-transverse momentum hadrons [32–34] and jets [35–37]) which are strongly suppressed as compared to p–p collisions. Thus, the leptons from W decays are valuable "messengers" from the initial state of heavy-ion collisions and could also be used to constrain the nPDFs [38–40].

In this paper, our main focus is on the centre-of-mass energy ($\sqrt{s}$) systematics of the production cross sections

[a] e-mail: francois.arleo@cern.ch

[b] e-mail: emilien.chapon@cern.ch

[c] e-mail: hannu.paukkunen@jyu.fi

---

[1] Unless a deuterium target, complicated by possible nuclear corrections, is used.

Springer

$d\sigma^{\ell\pm}/dy$ in hadronic collisions and the consequent scaling properties of the lepton charge asymmetry. First, in Sect. 2, we show how the scaling laws for absolute cross sections and charge asymmetries emerge from the relatively simple leading-order expressions. In Sect. 3 we then contrast these expectations against next-to-leading order (NLO) computations. Section 4 presents comparisons with the existing world data from LHC and Tevatron experiments as well as demonstrates how PDF uncertainties in some ratios of W cross sections can be suppressed by carefully choosing the rapidity binning. Finally, we summarise our main findings in Sect. 5.

2 Derivation of the scaling properties

2.1 Absolute cross sections

We consider the inclusive production of W bosons in high-energy collisions of two hadrons, H_1 and H_2, followed by the decay of W to a charged lepton and a neutrino,

$$H_1 + H_2 \rightarrow W^- + X \rightarrow \ell^- + \bar{\nu} + X,$$
$$H_1 + H_2 \rightarrow W^+ + X \rightarrow \ell^+ + \nu + X.$$

At leading order, the production cross section double differential in the charged lepton rapidity y and transverse momentum p_T reads [41,42],

$$
\frac{d^2\sigma^{\ell\pm}(s)}{dy\,dp_T} = \frac{\pi p_T}{24s^2}\left(\frac{\alpha_{em}}{\sin^2\theta_W}\right)^2 \sum_{i,j}\delta_{e_{q_i}+e_{\bar{q}_j},\pm 1}|V_{ij}|^2
$$
$$
\times \int_{x_2^{min}}^1 dx_2\left(x_2 - \frac{p_T}{\sqrt{s}}e^{-y}\right)^{-1}\frac{(x_1 x_2)^{-1}}{\left(x_1 x_2 s - M_W^2\right)^2 + M_W^2\Gamma_W^2}
$$
$$
\times\left[(\hat{t}+\hat{u}\pm\hat{t}\mp\hat{u})^2 q_i^{H_1}(x_1, Q^2)\bar{q}_j^{H_2}(x_2, Q^2)\right.
$$
$$
\left. + (\hat{t}+\hat{u}\mp\hat{t}\pm\hat{u})^2 \bar{q}_j^{H_1}(x_1, Q^2)q_i^{H_2}(x_2, Q^2)\right],
\tag{2}
$$

where the symbols α_{em}, θ_W, and V_{ij} refer to the fine-structure constant, the weak-mixing angle, and the elements of the Cabibbo–Kobayashi–Maskawa matrix, respectively. The mass and width of the W boson are denoted by M_W and Γ_W. The lower limit of the x_2 integral is given by $x_2^{min} = (p_T e^{-y})/(\sqrt{s} - p_T e^y)$ and the momentum argument $x_1 = (x_2 p_T e^y)/(x_2\sqrt{s} - p_T e^{-y})$. The Mandelstam variables $\hat{t}$ and $\hat{u}$ are

$$\hat{t} = -\sqrt{s}\,p_T x_1 e^{-y}, \quad \hat{u} = -\sqrt{s}\,p_T x_2 e^y. \tag{3}$$

The PDFs are denoted by $q_i^{H_k}(x, Q^2)$ (with $Q^2 = \mathcal{O}(M_W^2)$) and the sum runs over all flavours i, j such that the electric charges e_{q_i} of the quarks sum up to ± 1. Since the total width of the W boson is much smaller than its mass, $\Gamma_W \ll M_W$, we can make use of a delta-function identity $\epsilon/(x^2+\epsilon^2) \rightarrow \pi\delta(x)$, as $\epsilon \rightarrow 0$, to perform the remaining integral in Eq. (2).

We find

$$
\frac{d^2\sigma^{\ell\pm}(s)}{dy\,dp_T} \approx \frac{\pi^2}{24s}\left(\frac{\alpha_{em}}{\sin^2\theta_W}\right)^2\frac{1}{M_W\Gamma_W}
$$
$$
\times\frac{p_T}{\sqrt{1-4p_T^2/M_W^2}}\sum_{i,j}|V_{ij}|^2\,\delta_{e_{q_i}+e_{\bar{q}_j},\pm 1}
$$
$$
\times\left\{\left[1\mp\sqrt{1-4p_T^2/M_W^2}\right]^2 q_i^{H_1}(x_1^+)\bar{q}_j^{H_2}(x_2^+)\right.
$$
$$
+\left[1\pm\sqrt{1-4p_T^2/M_W^2}\right]^2 q_i^{H_1}(x_1^-)\bar{q}_j^{H_2}(x_2^-)
$$
$$
+\left[1\pm\sqrt{1-4p_T^2/M_W^2}\right]^2 \bar{q}_j^{H_1}(x_1^+)q_i^{H_2}(x_2^+)
$$
$$
\left.+\left[1\mp\sqrt{1-4p_T^2/M_W^2}\right]^2 \bar{q}_j^{H_1}(x_1^-)q_i^{H_2}(x_2^-)\right\},
\tag{4}
$$

where the momentum arguments of the PDFs are

$$x_1^\pm \equiv \frac{M_W^2 e^y}{2p_T\sqrt{s}}\left[1\mp\sqrt{1-4p_T^2/M_W^2}\right], \tag{5}$$

$$x_2^\pm \equiv \frac{M_W^2 e^{-y}}{2p_T\sqrt{s}}\left[1\pm\sqrt{1-4p_T^2/M_W^2}\right]. \tag{6}$$

Let us first consider a situation with[2] $y \gg 0$, that is, $x_2^\pm < x_1^\pm$. In terms of a dimensionless variable ξ_1 (which coincides with $x_1^\pm$ when $p_T \rightarrow M_W/2$),

$$\xi_1 \equiv \frac{M_W}{\sqrt{s}}e^y, \tag{7}$$

the momentum fractions in Eq. (6) become

$$x_1^\pm \equiv \frac{M_W}{2p_T}\xi_1\left[1\mp\sqrt{1-4p_T^2/M_W^2}\right], \tag{8}$$

$$x_2^\pm \equiv \frac{M_W^3}{2p_T s\xi_1}\left[1\pm\sqrt{1-4p_T^2/M_W^2}\right]. \tag{9}$$

At sufficiently small x, the sea-quark densities at high $Q^2 \sim M_W^2$ should be reasonably well approximated by a power law [43]

$$x\bar{q}_i(x, Q^2) \approx xq_i(x, Q^2) \approx N_i\,x^{-\alpha(Q^2)}, \tag{10}$$

where the exponent $\alpha(Q^2) > 0$ and the normalisations N_i should both be almost flavour independent. Such a behaviour (though not exactly a power law [44]) is expected by considering the small-x and large Q^2 limit (the so-called double logarithmic approximation [45]) of Dokshitzer–Gribov–Lipatov–Altarelli–Parisi parton evolution equations [46–52] and it is also consistent with the observations in deep inelastic scattering [53] with the Q^2 dependence of the exponent

---

[2] For simplicity, $y \gg 0$ ($y \ll 0$) should be understood as $e^y \gg 1$ ($e^y \ll 1$) in the remainder of the paper.

$\alpha(Q^2)$ being roughly logarithmic. However, in the following, the "running" of $\alpha(Q^2)$ does not directly show up since we will always set $Q^2 = M_W^2$. For brevity, we will denote $\alpha \equiv \alpha(Q^2 = M_W^2)$ from now on. By using the approximation Eq. (10) in Eq. (4) and trading the rapidity variable y with ξ_1, we find

$$\frac{d^2\sigma^{\ell^\pm}(s, \xi_1)}{dp_T d\xi_1} \approx s^\alpha \times f^\pm(\xi_1, p_T, H_1, H_2), \quad y \gg 0, \quad (11)$$

where $f^\pm(\xi, p_T, H_1, H_2)$ is a function that does not depend explicitly on s or y. Since the expression of Eq. (4) is peaked at $p_T \approx M_W/2$ and the p_T dependence of the probed momentum fractions in Eq. (6) is not particularly fierce, the x interval spanned by integration over p_T with a typical kinematic cut $p_T \gtrsim 20$ GeV remains sufficiently narrow such that approximation of Eq. (10) stays valid. Under these conditions, the scaling law in Eq. (11) holds also for p_T-integrated cross sections,

$$\frac{d\sigma^{\ell^\pm}(s, \xi_1)}{d\xi_1} \approx s^\alpha \times F^\pm(\xi_1, H_1, H_2), \quad y \gg 0, \quad (12)$$

where $F^\pm(\xi_1, H_1, H_2) \equiv \int dp_T f^\pm(\xi_1, p_T, H_1)\theta(p_T - p_T^{\min})$. In the backward direction with $y \ll 0$, the appropriate scaling variable is

$$\xi_2 \equiv \frac{M_W}{\sqrt{s}} e^{-y}, \quad (13)$$

such that

$$\frac{d\sigma^{\ell^\pm}(s, \xi_2)}{d\xi_2} \approx s^\alpha \times G^\pm(\xi_2, H_1, H_2), \quad y \ll 0, \quad (14)$$

where $G^\pm(\xi_2, H_1, H_2)$ is a function that does not depend explicitly on s or y. If $H_1 = H_2$, then $F^\pm(\xi_1, H_1, H_2) = G^\pm(\xi_2, H_1, H_2)$.

Here, we emphasise the fact that at fixed ξ_1 (ξ_2) the x region at which the PDFs of hadron H_1 (H_2) is sampled becomes approximately independent of $\sqrt{s}$; see Eq. (8). Going to forward (backward) direction pushes this region to large x where the parameterisation dependence of PDFs may be large. As a consequence, one could hope that the PDF uncertainties on cross-section ratios between two different values of $\sqrt{s}$ would better cancel out if performed at fixed $\xi_{1,2}$ than at fixed rapidity (as has been done e.g. by LHCb collaboration [16]). At small x, the probed x regions will be different for two different $\sqrt{s}$; see Eq. (9), but at large Q^2 the x dependence is almost purely dictated by the DGLAP evolution (in our scaling law approximated by a power law) and less prone to PDF uncertainties. We will come back to this later on in Sect. 4.2.

2.2 Charge asymmetries

Since the $\sqrt{s}$ dependence in Eqs. (12) and (14) is completely in the common prefactor s^α, it follows that the lepton charge-asymmetry equation (1) should obey a particularly simple scaling law,

$$\mathcal{C}_\ell^{H_1, H_2}(s, \xi_1) \approx F(\xi_1, H_1, H_2), \quad y \gg 0, \quad (15)$$
$$\mathcal{C}_\ell^{H_1, H_2}(s, \xi_2) \approx G(\xi_2, H_1, H_2), \quad y \ll 0,$$

where

$$F(\xi, H_1, H_2) \equiv \frac{F^+(\xi, H_1, H_2) - F^-(\xi, H_1, H_2)}{F^+(\xi, H_1, H_2) + F^-(\xi, H_1, H_2)}, \quad (16)$$

and similarly for G. In other words, at fixed ξ_1 or ξ_2, the charge asymmetry should be approximately independent of the centre-of-mass energy. In fact, here one can allow the exponent α to depend also on $\sqrt{s}$ and $\xi_{1,2}$ and it is only required that the PDFs are *locally* well approximated by a power law in the relevant region at small-x.

Another, and also a bit surprising feature of the charge asymmetry is that at sufficiently large $|y|$ it effectively depends only on the nucleon that is probed at large x. This follows from the facts that when $|y|$ is sufficiently large, either $u\bar{d}$ or $d\bar{u}$ partonic process eventually dominates, and that the light-sea-quark distributions are expected to be approximately SU(2) symmetric at small x,

$$u(x, Q^2) \approx \bar{u}(x, Q^2) \approx d(x, Q^2) \approx \bar{d}(x, Q^2), \quad x \ll 1, \quad (17)$$

and thus symmetric with respect to charge conjugation and isospin rotation. For example, one would expect that $\mathcal{C}_\ell^{p,p}(s, \xi_1) \approx \mathcal{C}_\ell^{p,\bar{p}}(s, \xi_1)$ at large ξ_1. In the case of nuclei the nPDFs $f_i^A(x, Q^2)$ are built from the free nucleon PDFs $f_i^{\text{proton}}(x, Q^2)$ and nuclear modification factors $R_i^{\text{proton}, A}$ by (see e.g. [26])

$$f_i^A(x, Q^2) = Z f_i^{\text{proton}, A}(x, Q^2) + N f_i^{\text{neutron}, A}(x, Q^2), \quad (18)$$

where

$$f_i^{\text{proton}, A}(x, Q^2) = R_i^{\text{proton}, A} f_i^{\text{proton}}(x, Q^2), \quad (19)$$
$$f_i^{\text{neutron}, A}(x, Q^2) = f_{i, u \leftrightarrow d}^{\text{proton}, A}(x, Q^2). \quad (20)$$

At small-x one expects modest shadowing ($R_i^{\text{proton}, A} < 1$), which, however, should not significantly alter the scaling exponent α (particularly at high $Q^2 \sim M_W^2$ involved here) and, to a good approximation, the effect of shadowing is just a slight overall downward normalisation in the absolute cross sections which should largely disappear in the case of charge asymmetry. In other words, we can encapsulate the scaling law for lepton charge asymmetry as
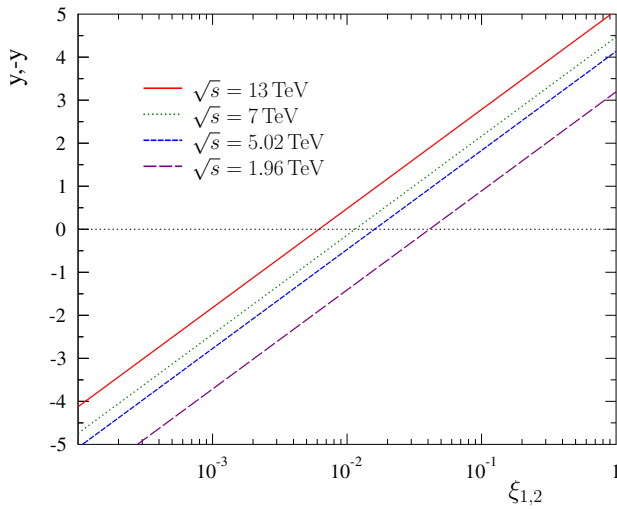
Fig. 1 Relation of rapidity y and scaling variables $\xi_{1,2}$ for a few values of $\sqrt{s}$

$$\mathcal{C}_{\ell}^{\mathrm{H_1,H_2}}(s, \xi_1) \approx F(\xi_1, \mathrm{H_1}), \quad y \gg 0,$$
$$\mathcal{C}_{\ell}^{\mathrm{H_1,H_2}}(s, \xi_2) \approx G(\xi_2, \mathrm{H_2}), \quad y \ll 0, \quad (21)$$

independently of the nature of hadron (nucleon, anti-nucleon, nucleus) probed at small x.

3 Scaling vs. NLO calculation

Most of our plots in the rest of the paper will use the scaling variables $\xi_{1,2}$, which are related to the rapidity y and centre-of-mass energy $\sqrt{s}$ via Eqs. (7) and (13). To ease the interpretation in what follows, this dependence is illustrated in Fig. 1.

According to Eq. (10), the scaling exponent α in Eq. (12) should reflect the small-x behaviour of quark distributions and it can be straightforwardly extracted from cross sections at two different centre-of-mass energies. To verify this correspondence and the consistency of our derivation, we have computed the full NLO cross sections at $\sqrt{s} = 7, 8, 13$ TeV for p–p collisions using MCFM Monte-Carlo code [54] and CT10NLO PDFs [22]. From these cross sections, we have evaluated the effective scaling exponent α_{eff} by

$$\alpha_{\mathrm{eff}}(\xi) = \log \left[\frac{\sigma^{\ell^\pm}(s, \xi)/d\xi}{\sigma^{\ell^\pm}(s', \xi)/d\xi} \right] \log^{-1} \left(\frac{s}{s'} \right), \quad (22)$$

taking $\sqrt{s} = 7$ TeV and $\sqrt{s'} = 8, 13$ TeV. The outcome is plotted in the upper panel of Fig. 2. To first approximation, toward large $\xi_{1,2}$ the effective scaling exponent is $\alpha_{\mathrm{eff}} \approx 0.35$ and independent of the lepton charge. In more detail, the scaling exponent is not exactly constant but some variation is visible which reflects the fact that the PDFs do not follow a pure power law, especially when x is not very small
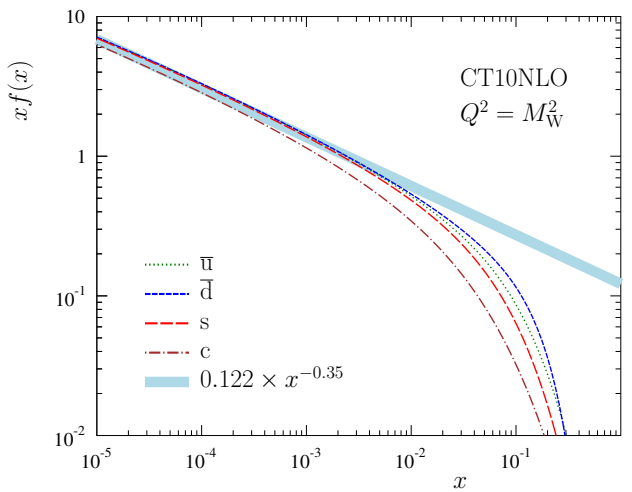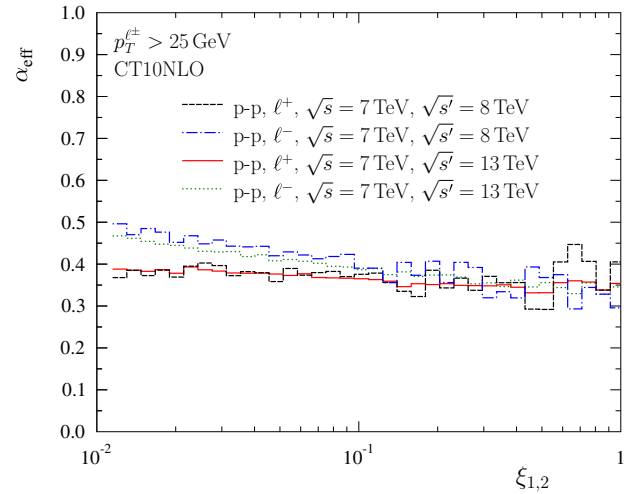

Fig. 2 Scaling exponent extracted from NLO calculations (*upper panel*) and its comparison with CT10NLO PDFs (*lower panel*)

(at small $\xi_{1,2}$). The scaling exponent for ℓ^- tends to have more slope and to be somewhat larger than that of ℓ^+ especially at small $\xi_{1,2}$, which corresponds to midrapidity. This can be explained by the slightly steeper slope of the $\bar{u}$ distribution in comparison to $\bar{d}$ distribution (see the lower panel of Fig. 2) and the fact that ℓ^- production tends to be sensitive to somewhat larger values of x in the small-x side. The latter follows from the factors $(1 \pm \sqrt{1 - 4p_{\mathrm{T}}^2/M_{\mathrm{W}}^2})^2$ that multiply PDFs in Eq. (4). These, in turn, originate from the parity non-conserving W couplings to quarks and leptons. The lower panel in Fig. 2 compares the extracted exponent $\alpha_{\mathrm{eff}} \approx 0.35$ to the CT10NLO sea-quark PDFs. Evidently, there is a good correspondence between the scaling exponent α and the behaviour of the small-x quark PDFs. We can conclude that despite the complex higher-order QCD calculations, the centre-of-mass dependence of the cross sections being discussed can be essentially captured by a simple power law.
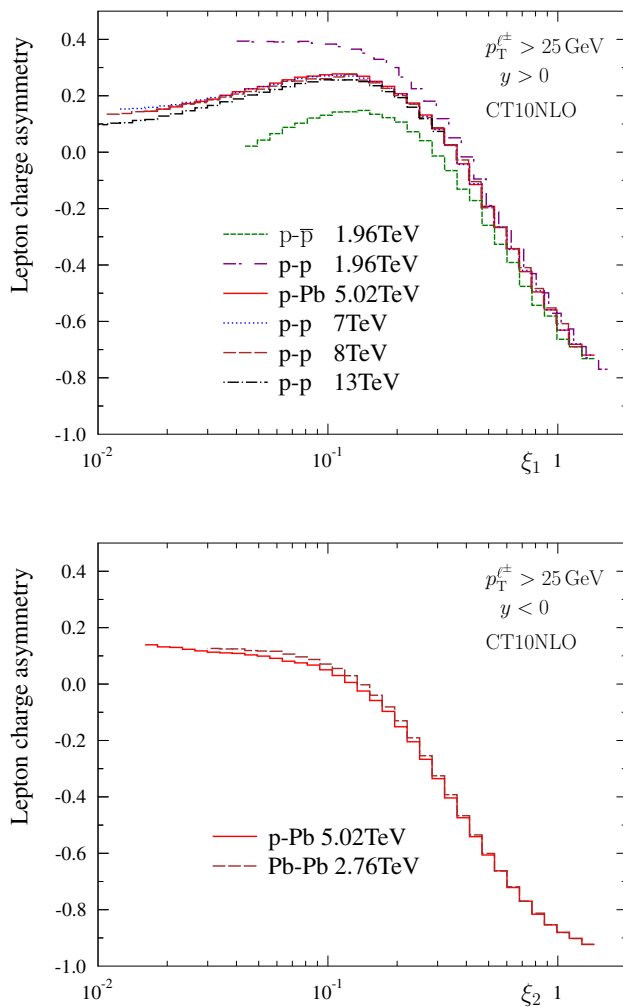
Fig. 3 Lepton charge asymmetry in p–p̄ ($\sqrt{s}$ = 1.96 TeV), p–p ($\sqrt{s}$ = 1.96, 7, 8 TeV), p–Pb ($\sqrt{s}$ = 5.02 TeV) and Pb–Pb ($\sqrt{s}$ = 2.76 TeV) collisions, for $y > 0$ (*upper panel*) and $y < 0$ (*lower panel*)

Let us now discuss Eq. (21) and whether the nature of the hadronic projectile or nucleus probed at small x really disappears as conjectured. To this end we have computed the lepton charge asymmetry (again, at NLO accuracy) in various collision systems at centre-of-mass energies that correspond to existing Tevatron and LHC data. The results are shown in Fig. 3. At $y \gg 0$, the curves corresponding to p–p, p–Pb and p–p̄ tend to unite, whereas in the opposite direction, $y \ll 0$, p–Pb and Pb–Pb become approximately the same. Thus, as far as theoretical NLO expectations are concerned, the scaling law of Eq. (21) turns out to be a very good approximation, though not perfect. The largest deviations in Fig. 3 are seen in the case of p–p̄ at the Tevatron energy, $\sqrt{s}$ = 1.96 TeV. There, the probed values of x for p̄ are not small enough and especially the assumption of charge-conjugation symmetric quark distributions, Eq. (17), is not particularly accurate until almost the end of phase space (e.g. $\xi_1 = 1$ corresponds to

$x_2 \approx M_W^2/s \approx 0.002$). The p–p curve at the same centre-of-mass energy unites with the rest already at lower ξ_1.

At small fixed value of ξ, the lepton charge asymmetry in p–p collisions tends to decrease toward increasing centre-of-mass energies. This can be interpreted in terms of the slightly different scaling exponent for ℓ^+ and ℓ^- production (see Fig. 2). Denoting the scaling exponent for $\ell^\pm$ production by $\alpha^\pm$, and the difference by $\Delta \equiv \alpha^- - \alpha^+$, to a first approximation,

$$\mathcal{C}_\ell^{H_1,H_2}(s',\xi) = \mathcal{C}_\ell^{H_1,H_2}(s,\xi)$$
$$+ \frac{\Delta}{2}\left\{1 - \left[\mathcal{C}_\ell^{H_1,H_2}(s,\xi)\right]^2\right\}\log\left(\frac{s}{s'}\right) + \mathcal{O}(\Delta^2). \quad (23)$$

Since $\Delta > 0$, we have a condition

$$\mathcal{C}_\ell^{H_1,H_2}(s',\xi) < \mathcal{C}_\ell^{H_1,H_2}(s,\xi), \quad \text{if } s' > s, \quad (24)$$

which explains the decreasing trend of lepton charge asymmetries in p–p collisions toward higher centre-of-mass energies at fixed, small ξ.

4 Data and predictions

4.1 Comparison with existing data

The currently most accurate experimental measurements for inclusive W production from Tevatron and LHC experiments are summarised in Table 1. A direct comparison of various measurements is complicated by the kinematic cuts for lepton p_T, missing transverse energy $\not{E}_T$, and transverse mass m_T of the neutrino–lepton system, which vary among the experiments and have to be accounted for. Here, we have chosen to "correct" the data to $p_T > 25$ GeV (the default cut in CMS measurements) by MCFM evaluating the observables first with the true cuts shown in Table 1, then with $p_T > 25$ GeV and taking the ratio (absolute cross sections) or difference (charge asymmetry). We stress that if the kinematic cuts were the same in all experiments, this step would be unnecessary. The available absolute cross sections are compared in Fig. 4. The p–p and p–Pb data are plotted together at forward rapidity (left-hand panels) and Pb–Pb and p–Pb data together at backward rapidity (right-hand panels). In these plots, the data has been scaled by a factor $(s/\text{GeV}^2)^{-\alpha}$, where a constant value $\alpha = 0.4$ has been used for the scaling exponent as a compromise between the expected exponent at small and large ξ; see Fig. 2. Keeping in mind the "non-constantness" of the scaling exponent and that at forward (backward) direction the p–Pb (Pb–Pb) data are presumably affected by small-x shadowing in comparison to p–p (p–Pb), an exact match with p–p (p–Pb) is not expected. Nevertheless, there is clearly a rough correspondence between the data from different collision systems and different $\sqrt{s}$.

Table 1 The experimental data sets

Experiment	System	$\sqrt{s}$ (TeV)	Kinematic cuts	Refs.
D0	p–$\bar{\text{p}}$	1.96	$p_T > 25$ GeV, $\not{E}_T > 25$ GeV	[10]
ATLAS	Pb–Pb	2.76	$p_T > 25$ GeV, $\not{E}_T > 25$ GeV, $m_T > 40$ GeV	[30]
CMS	p–Pb	5.02	$p_T > 25$ GeV	[23]
ALICE	p–Pb	5.02	$p_T > 10$ GeV	[24]
CMS	p–p	7	$p_T > 25$ GeV	[13]
ATLAS	p–p	7	$p_T > 20$ GeV, $\not{E}_T > 25$ GeV, $m_T > 40$ GeV	[55]
LHCb	p–p	7	$p_T > 20$ GeV	[15]
LHCb	p–p	8	$p_T > 20$ GeV	[16]
CMS	p–p	8	$p_T > 25$ GeV	[14]
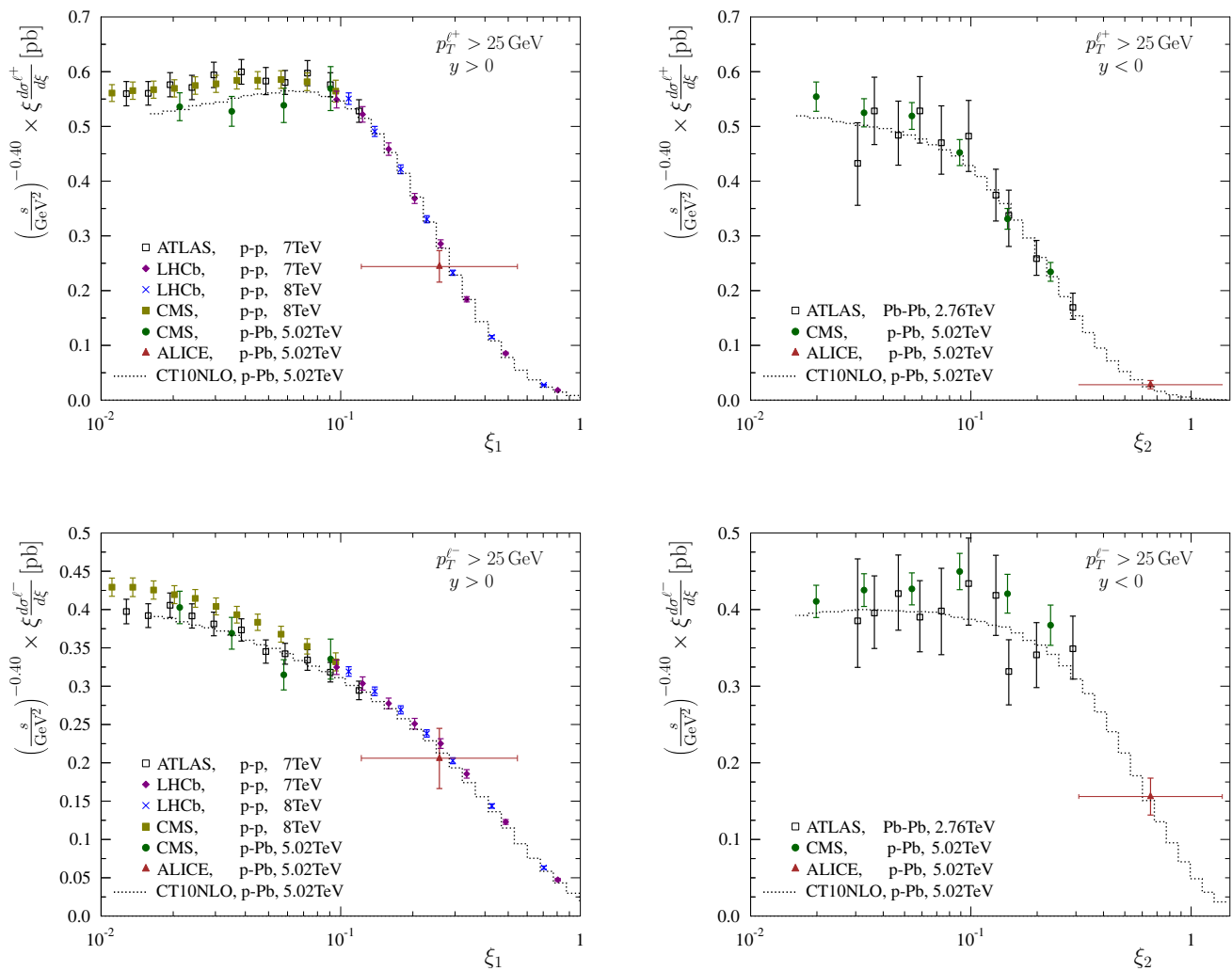
Fig. 4 Absolute spectra of charged leptons (*upper panels* for ℓ^+, *lower panels* for ℓ^-) in p–p ($\sqrt{s} = 7, 8$ TeV) and p–Pb ($\sqrt{s} = 5.02$ TeV) collisions for $y > 0$ (*left-hand panels*), and in Pb–Pb ($\sqrt{s} = 2.76$ TeV) and p–Pb ($\sqrt{s} = 5.02$ TeV) collisions for $y < 0$. The data has been scaled by $(s/\text{GeV}^2)^{-0.40}$

The data for lepton charge asymmetries $\mathcal{C}_\ell$ are compiled in Fig. 5. We note that some experimental uncertainties, luminosity above all, cancel in the measurement of the lepton charge asymmetries as compared to absolute cross sections. As previously, the data from p–p, p–$\bar{\text{p}}$, and Pb–Pb collisions are plotted only in the direction where they are supposed
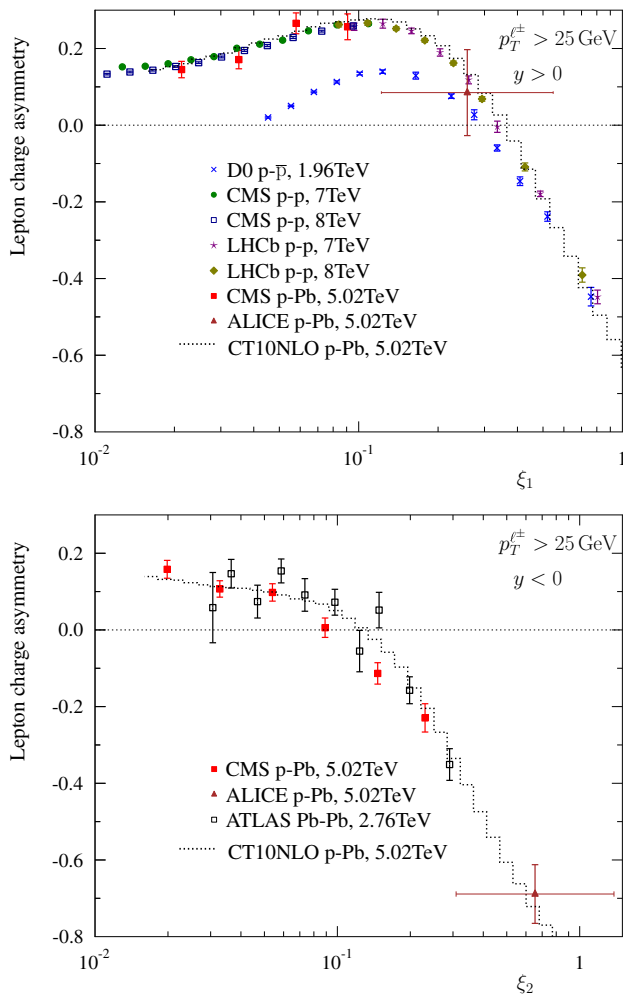
Fig. 5 Lepton charge asymmetry in p–p̄ ($\sqrt{s} = 1.96$ TeV), p–p ($\sqrt{s} = 7, 8$ TeV), p–Pb ($\sqrt{s} = 5.02$ TeV) and Pb–Pb ($\sqrt{s} = 2.76$ TeV) collisions. *The dotted curve* is to guide the eye and corresponds to $\mathcal{C}_\ell^{\mathrm{p,Pb}}$ at $\sqrt{s} = 5.02$ TeV

Fig. 6 The world data on lepton charge asymmetry as a function of y_{ref} taking $\sqrt{s_{\mathrm{ref}}} = 5.02$ TeV

$$y_{\mathrm{ref}} \equiv y \pm \frac{1}{2} \log \frac{s_{\mathrm{ref}}}{s}, \quad y \gtrless 0, \tag{25}$$

such that

$$\xi_1(y, \sqrt{s}) = \xi_1(y_{\mathrm{ref}}, \sqrt{s_{\mathrm{ref}}}), \quad y > 0, \tag{26}$$
$$\xi_2(y, \sqrt{s}) = \xi_2(y_{\mathrm{ref}}, \sqrt{s_{\mathrm{ref}}}), \quad y < 0.$$

Such a plot is shown in Fig. 6. In order to keep the plot readable Pb–Pb data is plotted only at $y < 0$, and p–p, p–p̄ data is plotted only at $y > 0$.

4.2 Cross-section ratios

In Sect. 2.1 we noted that the ratios of cross sections at two nearby $\sqrt{s}$ at fixed values of scaling variable $\xi_{1,2}$ could become less prone to large-x PDF uncertainties in comparison to taking the ratios at fixed rapidity. To investigate this statement quantitatively, we have computed (p–p collisions, NLO precision) ratios

$$R^+_{\sqrt{s'}/\sqrt{s}}(y_{\mathrm{ref}}) = \frac{\mathrm{d}\sigma^{\ell^+}(\sqrt{s'})/\mathrm{d}y_{\mathrm{ref}}}{\mathrm{d}\sigma^{\ell^+}(\sqrt{s})/\mathrm{d}y_{\mathrm{ref}}} \approx \left(\frac{\sqrt{s'}}{\sqrt{s}}\right)^{2\alpha}, \tag{27}$$

$$R^-_{\sqrt{s'}/\sqrt{s}}(y_{\mathrm{ref}}) = \frac{\mathrm{d}\sigma^{\ell^-}(\sqrt{s'})/\mathrm{d}y_{\mathrm{ref}}}{\mathrm{d}\sigma^{\ell^-}(\sqrt{s})/\mathrm{d}y_{\mathrm{ref}}} \approx \left(\frac{\sqrt{s'}}{\sqrt{s}}\right)^{2\alpha}, \tag{28}$$

$$R_{\sqrt{s'}/\sqrt{s}}(y_{\mathrm{ref}}) = \frac{R^+_{\sqrt{s'}/\sqrt{s}}(y_{\mathrm{ref}})}{R^-_{\sqrt{s'}/\sqrt{s}}(y_{\mathrm{ref}})} \approx 1, \tag{29}$$

where the predictions from scaling laws are also indicated. For comparison we evaluate the same ratios also at fixed rapidity (instead of fixed y_{ref}). We have used `PDF4LHC15_30NLO` set of PDFs [56] available from the LHAPDF library [57]. This is a hybrid set that combines [58] information from independent PDF fits (CT14 [59],

to merge with p–Pb data. To a very good approximation, the experimental data indeed line up to the same underlying curve which corresponds to the charge asymmetry in p–Pb collisions. Two CMS p–Pb data points at negative rapidities appear to lie below the NLO predictions and could potentially require additional nuclear modifications in PDFs (as also pointed out in Ref. [23]). However, the ATLAS Pb–Pb data shows no sign of such a disagreement with the theory at those values of rapidity indicating that there appears to be some tension between these two data sets and that the both data sets cannot be optimally reproduced with the same set of (nuclear) PDFs.

We can also compress all the data into a single plot. This is done by choosing a certain reference centre-of-mass energy $\sqrt{s_{\mathrm{ref}}}$ (we take $\sqrt{s_{\mathrm{ref}}} = 5.02$ TeV) and plotting the data as a function of variable
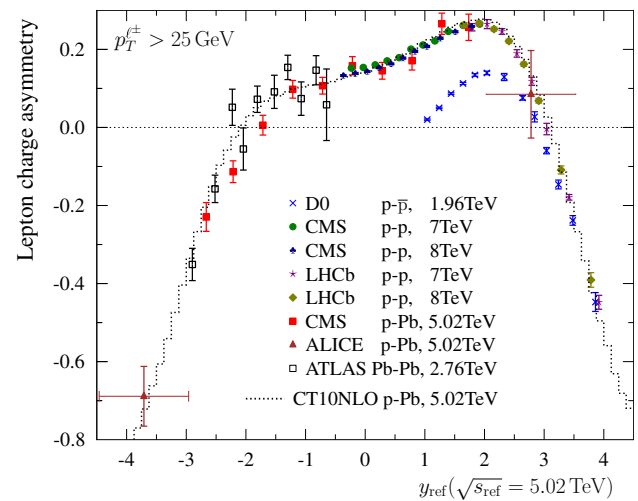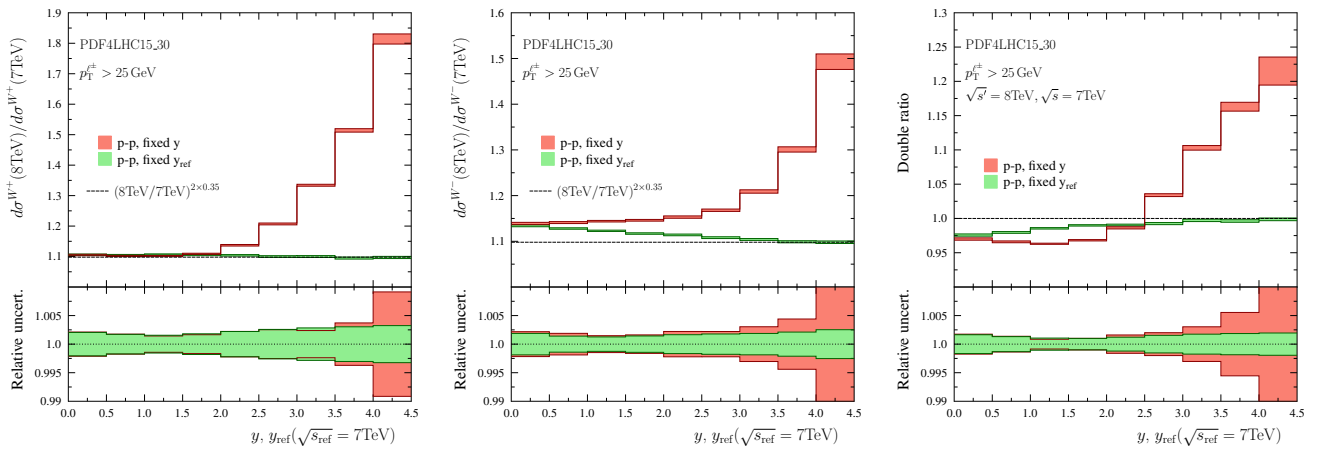
Fig. 7 Ratios of ℓ^+ (*left*) and ℓ^- (*middle*) spectra computed at $\sqrt{s} = 8$ TeV and $\sqrt{s} = 7$ TeV centre-of-mass energies. In *red color* are the results binned in lepton rapidity y, and in *green* the results binned in y_{ref} taking $\sqrt{s_{ref}} = 7$ TeV. *The dashed lines* indicate the prediction of scaling law Eq. (12). *The right-hand panel* shows the double ratio of Eq. (27)
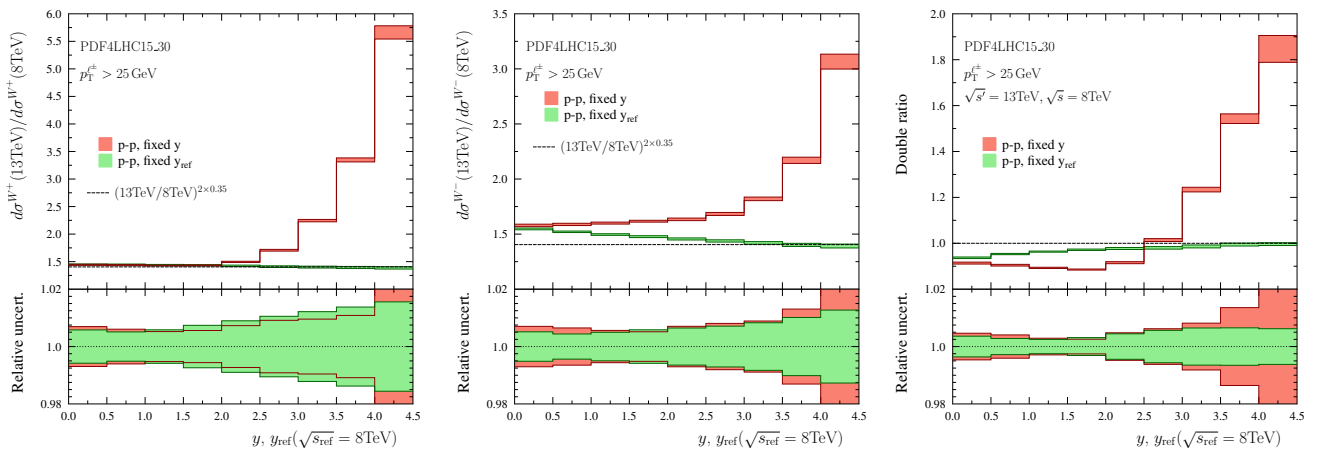

Fig. 8 As Fig. 7 but using $\sqrt{s'} = 13$ TeV and $\sqrt{s} = 8$ TeV

MMHT14 [60], NNPDF3.0 [61]) thereby giving a better idea of the uncertainties than when sticking to a one particular PDF provider.

The results are shown in Fig. 7 ($\sqrt{s'} = 8$ TeV, $\sqrt{s} = 7$ TeV), Fig. 8 ($\sqrt{s'} = 13$ TeV, $\sqrt{s} = 8$ TeV), and Fig. 9 ($\sqrt{s'} = 14$ TeV, $\sqrt{s} = 13$ TeV). The histograms in red indicate the outcome when the ratios are taken at fixed rapidity intervals and the green ones correspond to making the ratios at fixed y_{ref} (equivalent to fixed ξ_1). One can observe that in the case of W^- production and the double ratio the PDF uncertainties indeed tend to cancel out better when the ratios are taken at fixed y_{ref}. For W^+ production it appears that there is no definite advantage (in the sense that PDF uncertainties would decrease) in binning as a function of y_{ref}. We attribute this to the fact that in the case of W^+, the integrand (in Eq. (4)) in x is broader for W^+ production than what it is for W^- production and the PDF uncertainties do not cancel as effectively.

The LHCb collaboration has recently reported [16] ratios similar to ones discussed here (though integrated over the rapidity interval $2 < y < 4.5$), and has observed some deviations between the measurements and NLO calculations. Our results suggest that by making the rapidity intervals equal in y_{ref}, the PDF uncertainties especially in the double ratio can be suppressed and the significance of the measurement thereby increased.[3]

5 Summary

We have discussed the scaling properties of inclusive charged leptons from decays of W bosons created in hadronic

---

[3] An even better precision could be attained by considering the ratios of *total* cross sections [62], which, however, are more difficult to measure for the finite acceptance of the experimental apparatuses.
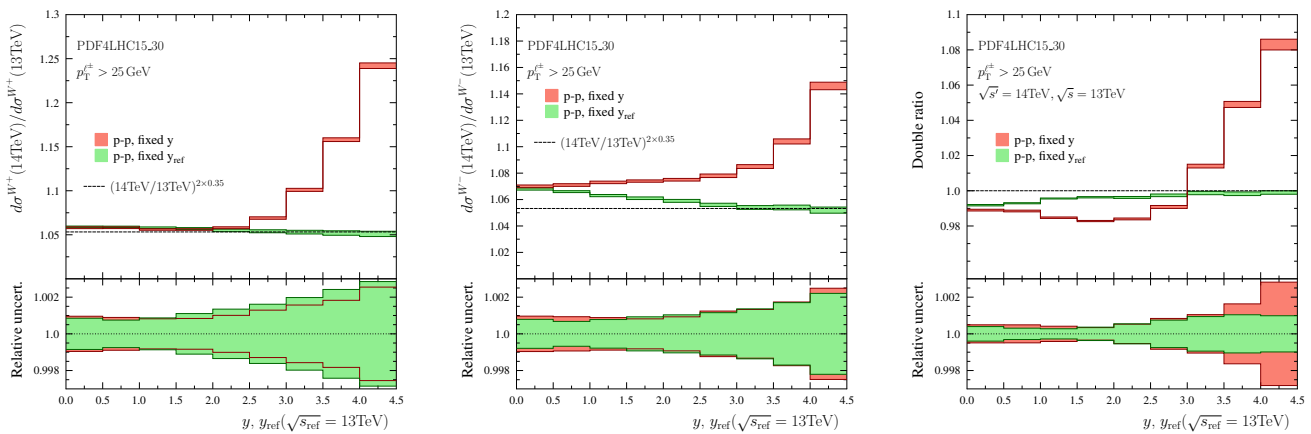
Fig. 9 As Fig. 7 but using $\sqrt{s'} = 14$ TeV and $\sqrt{s} = 13$ TeV

collisions. Based on the leading-order estimate, we have found that the $\sqrt{s}$ dependence of cross sections in forward/backward directions at fixed value of the scaling variable $\xi_{1,2} = (M_W/\sqrt{s})e^{\pm y}$ should approximately obey a one-parameter power law, in which the scaling exponent is approximately independent of the lepton charge and reflects the slope of the small-x PDFs. Consequently, the lepton charge asymmetries at different centre-of-mass energies are predicted to be approximately same at fixed $\xi_{1,2}$. Moreover, lepton charge asymmetries in different collision systems are related: at large positive (negative) y the lepton charge asymmetry depends effectively only on the nature of the forward-(backward-) going nucleon or nucleus. A comparison with the experimental data from LHC and Tevatron confirms that the derived scaling laws are indeed able to capture very well the behaviour of the data.

While these scaling laws by no means serve as a replacement for accurate (NLO and beyond) calculations, the possibility of a direct comparison of various data should be useful in e.g. checking the mutual compatibility since by fixing ξ_1 (ξ_2) one forces the PDFs to be sampled at approximately the same regions of x_1 (x_2) independently of $\sqrt{s}$. This, as we demonstrated, can in turn be taken advantage of by reducing PDF uncertainties in ratios of cross sections measured at different $\sqrt{s}$. This could increase the sensitivity of the experiments e.g. to possible contributions from physics beyond the Standard Model.

References

1. M.L. Mangano, arXiv:1512.00220 [hep-ph]
2. E.L. Berger, F. Halzen, C.S. Kim, S. Willenbrock, Phys. Rev. D **40**, 83 (1989)
3. E.L. Berger, F. Halzen, C.S. Kim, S. Willenbrock, Phys. Rev. D **40**, 3789 (1989)
4. A.D. Martin, R.G. Roberts, W.J. Stirling, Mod. Phys. Lett. A **4**, 1135 (1989)
5. F. Abe et al. (CDF Collaboration), Phys. Rev. Lett. **81**, 5754 (1998). arXiv:hep-ex/9809001
6. D. Acosta et al. (CDF Collaboration), Phys. Rev. D **71**, 051104 (2005). arXiv:hep-ex/0501023
7. V.M. Abazov et al. (D0 Collaboration), Phys. Rev. Lett. **101**, 211801 (2008). arXiv:0807.3367 [hep-ex]
8. V.M. Abazov et al. (D0 Collaboration), Phys. Rev. D **77** (2008) 011106. arXiv:0709.4254 [hep-ex]
9. V.M. Abazov et al. (D0 Collaboration), Phys. Rev. D **88**, 091102 (2013). arXiv:1309.2591 [hep-ex]
10. V.M. Abazov et al. (D0 Collaboration), Phys. Rev. D **91**(3), 032007 (2015). arXiv:1412.2862 [hep-ex]
11. G. Aad et al. (ATLAS Collaboration), JHEP **1012**, 060 (2010). arXiv:1010.2130 [hep-ex]
12. G. Aad et al. (ATLAS Collaboration), Phys. Lett. B **701**, 31 (2011). arXiv:1103.2929 [hep-ex]
13. S. Chatrchyan et al. (CMS Collaboration), Phys. Rev. D **90**(3), 032004 (2014). arXiv:1312.6283 [hep-ex]
14. V. Khachatryan et al. (CMS Collaboration), arXiv:1603.01803 [hep-ex]
15. R. Aaij et al. (LHCb Collaboration), JHEP **1412**, 079 (2014). arXiv:1408.4354 [hep-ex]
16. R. Aaij et al. (LHCb Collaboration), JHEP **1601**, 155 (2016). arXiv:1511.08039 [hep-ex]
17. C. Anastasiou, L.J. Dixon, K. Melnikov, F. Petriello, Phys. Rev. D **69**, 094008 (2004). arXiv:hep-ph/0312266
18. S. Catani, L. Cieri, G. Ferrera, D. de Florian, M. Grazzini, Phys. Rev. Lett. **103**, 082001 (2009). arXiv:0903.2120 [hep-ph]
19. R.D. Ball et al. (NNPDF Collaboration), Nucl. Phys. B **849**, 112 (2011)
20. R.D. Ball et al. (NNPDF Collaboration), Nucl. Phys. B **854**, 926 (2012)

21. R.D. Ball et al. (NNPDF Collaboration), Nucl. Phys. B **855** (2012) 927. arXiv:1012.0836 [hep-ph]

22. H.L. Lai, M. Guzzi, J. Huston, Z. Li, P.M. Nadolsky, J. Pumplin, C.-P. Yuan, Phys. Rev. D **82**, 074024 (2010). arXiv:1007.2241 [hep-ph]

23. V. Khachatryan et al. (CMS Collaboration), Phys. Lett. B **750**, 565 (2015). doi:10.1016/j.physletb.2015.09.057. arXiv:1503.05825 [nucl-ex]

24. J. Zhu (ALICE Collaboration), J. Phys. Conf. Ser. **612**(1), 012009 (2015)

25. The ATLAS collaboration, ATLAS-CONF-2015-056

26. K.J. Eskola, H. Paukkunen, C.A. Salgado, JHEP **0904**, 065 (2009). arXiv:0902.4154 [hep-ph]

27. M. Hirai, S. Kumano, T.-H. Nagai, Phys. Rev. C **76**, 065207 (2007). arXiv:0709.3038 [hep-ph]

28. K. Kovarik et al., arXiv:1509.00792 [hep-ph]

29. D. de Florian, R. Sassot, P. Zurita, M. Stratmann, Phys. Rev. D **85**, 074028 (2012). arXiv:1112.6324 [hep-ph]

30. G. Aad et al. (ATLAS Collaboration), Eur. Phys. J. C **75**(1), 23 (2015). arXiv:1408.4674 [hep-ex]

31. S. Chatrchyan et al. (CMS Collaboration), Phys. Lett. B **715**, 66 (2012). arXiv:1205.6334 [nucl-ex]

32. S. Chatrchyan et al. (CMS Collaboration), Eur. Phys. J. C **72**, 1945 (2012). arXiv:1202.2554 [nucl-ex]

33. G. Aad et al. (ATLAS Collaboration), JHEP **1509**, 050 (2015). doi:10.1007/JHEP09(2015)050. arXiv:1504.04337 [hep-ex]

34. B.B. Abelev et al. (ALICE Collaboration), Phys. Lett. B **736**, 196 (2014). arXiv:1401.1250 [nucl-ex]

35. CMS Collaboration [CMS Collaboration], CMS-PAS-HIN-12-004

36. G. Aad et al. (ATLAS Collaboration), Phys. Rev. Lett. **114**(7), 072302 (2015). arXiv:1411.2357 [hep-ex]

37. J. Adam et al. (ALICE Collaboration), Phys. Lett. B **746**, 1 (2015). arXiv:1502.01689 [nucl-ex]

38. H. Paukkunen, C.A. Salgado, JHEP **1103**, 071 (2011). arXiv:1010.5392 [hep-ph]

39. P. Ru, B.W. Zhang, L. Cheng, E. Wang, W.N. Zhang, J. Phys. G **42**(8), 085104 (2015). doi:10.1088/0954-3899/42/8/085104. arXiv:1412.2930 [nucl-th]

40. P. Ru, B.W. Zhang, E. Wang, W.N. Zhang, Eur. Phys. J. C **75**(9), 426 (2015). doi:10.1140/epjc/s10052-015-3652-x. arXiv:1505.08106 [nucl-th]

41. P. Aurenche, J. Lindfors, Nucl. Phys. B **185**, 274 (1981)

42. H. Baer, M.H. Reno, Phys. Rev. D **43**, 2892 (1991)

43. M. Gluck, E. Reya, A. Vogt, Eur. Phys. J. C **5**, 461 (1998). arXiv:hep-ph/9806404

44. R.D. Ball, S. Forte, Phys. Lett. B **335**, 77 (1994). doi:10.1016/0370-2693(94)91561-X. arXiv:hep-ph/9405320

45. L.V. Gribov, E.M. Levin, M.G. Ryskin, Nucl. Phys. B **188**, 555 (1981)

46. Y.L. Dokshitzer, Sov. Phys. JETP **46**, 641 (1977)

47. Y.L. Dokshitzer, Zh. Eksp. Teor. Fiz. **73**, 1216 (1977)

48. V.N. Gribov, L.N. Lipatov, Sov. J. Nucl. Phys. **15**, 438 (1972)

49. V.N. Gribov, L.N. Lipatov, Yad. Fiz. **15**, 781 (1972)

50. V.N. Gribov, L.N. Lipatov, Sov. J. Nucl. Phys. **15**, 675 (1972)

51. V.N. Gribov, L.N. Lipatov, Yad. Fiz. **15**, 1218 (1972)

52. G. Altarelli, G. Parisi, Nucl. Phys. B **126**, 298 (1977)

53. C. Adloff et al. (H1 Collaboration), Phys. Lett. B **520**, 183 (2001). arXiv:hep-ex/0108035

54. J.M. Campbell, R.K. Ellis, Nucl. Phys. Proc. Suppl. **205–206**, 10 (2010). arXiv:1007.3492 [hep-ph]

55. G. Aad et al. (ATLAS Collaboration), Phys. Rev. D **85**, 072004 (2012). arXiv:1109.5141 [hep-ex]

56. J. Butterworth et al., J. Phys. G **43**, 023001 (2016). doi:10.1088/0954-3899/43/2/023001. arXiv:1510.03865 [hep-ph]

57. A. Buckley, J. Ferrando, S. Lloyd, K. Nordstrm, B. Page, M. Rfenacht, M. Schnherr, G. Watt, Eur. Phys. J. C **75**, 132 (2015). doi:10.1140/epjc/s10052-015-3318-8. arXiv:1412.7420 [hep-ph]

58. J. Gao, P. Nadolsky, JHEP **1407**, 035 (2014). doi:10.1007/JHEP07(2014)035. arXiv:1401.0013 [hep-ph]

59. S. Dulat et al., Phys. Rev. D **93**, 033006 (2016). arXiv:1506.07443 [hep-ph]

60. L.A. Harland-Lang, A.D. Martin, P. Motylinski, R.S. Thorne, Eur. Phys. J. C **75**(5), 204 (2015). arXiv:1412.3989 [hep-ph]

61. R.D. Ball et al. (NNPDF Collaboration), JHEP **1504**, 040 (2015). doi:10.1007/JHEP04(2015)040. arXiv:1410.8849 [hep-ph]

62. M.L. Mangano, J. Rojo, JHEP **1208**, 010 (2012). arXiv:1206.3557 [hep-ph]